AGU PUBLICATIONS

Geochemistry, Geophysics, Geosystems

RESEARCH ARTICLE
10.1002/2016GC006794

Aluminum in zircon as evidence for peraluminous and metaluminous melts from the Hadean to present

Dustin Trail[1], Nicholas Tailby[2], Yanling Wang[1], T. Mark Harrison[3], and Patrick Boehnke[3,4]

[1]Department of Earth and Environmental Sciences, University of Rochester, Rochester, New York, USA, [2]Department of Earth and Planetary Sciences, American Museum of Natural History, New York, New York, USA, [3]Department of Earth, Planetary, and Space Sciences, University of California, Los Angeles, California, USA, [4]Now at Department of the Geophysical Sciences, University of Chicago, Chicago, Illinois, USA

Key Points:
- Approximately 800 Al concentrations in zircons measured in 19 different peraluminous and metaluminous rocks
- Al concentrations in zircons from peraluminous rocks are distinctly higher than zircons from metaluminous rocks
- Al in zircon proposed as a tool to discriminate peraluminous and metaluminous rocks within the detrital zircon record

Supporting Information:
- Supporting Information S1
- Figure S1
- Table S1
- Table S2
- Table S3
- Table S4

Correspondence to:
D. Trail,
dtrail@ur.rochester.edu

Citation:
Trail, D., N. Tailby, Y. Wang, T. Mark Harrison, and P. Boehnke (2017), Aluminum in zircon as evidence for peraluminous and metaluminous melts from the Hadean to present, *Geochem. Geophys. Geosyst.*, *18*, 1580–1593, doi:10.1002/2016GC006794.

Received 30 DEC 2016
Accepted 26 MAR 2017
Accepted article online 3 APR 2017
Published online 18 APR 2017

Abstract Zircon structurally accommodates a range of trace impurities into its lattice, a feature which is used extensively to investigate the evolution of silicate magmas. One key compositional boundary of magmas is defined by whether the molar ratio of $Al_2O_3/(CaO + Na_2O + K_2O)$ is larger or smaller than unity. Here we report ~800 Al in zircon concentrations from 19 different rocks from the Lachlan Fold Belt (southeastern Australia), New England (USA), and Arunachal leucogranites (eastern Himalaya) with $Al_2O_3/(CaO + Na_2O + K_2O)$ whole rock values that range from 0.88 to 1.6. Zircons from peraluminous rocks yield an average Al concentration of ~10 ppm, which distinguishes them from crystals found in metaluminous rocks (~1.3 ppm). This difference is related to the materials involved in the melting, assimilation, and/or magma differentiation processes; for example, magmas that assimilate Al-rich material such as metapelites are expected to produce melts with elevated alumina activities, and thus zircons with high Al concentrations. These observations are applied to the Archean and Hadean Jack Hills detrital zircon record. Detrital Archean zircons, with ages from about 3.30 to 3.75 Ga, yield Al in zircon concentrations consistent with origins in peraluminous rocks in ~8% of the cases (n = 236). A single zircon from the pre-3.9 Ga age group (n = 39) contains elevated Al contents, which suggests that metaluminous crustal rocks were more common than peraluminous rocks in the Hadean. Weathered material assimilated into these Hadean source melts was not dominated by Al-rich source material.

1. Introduction

The majority of granitoid magmas are generated by partial melting within the crust. Many of the original source rocks remain unexposed, leading researchers to investigate the chemical and isotopic information of the resulting granites themselves, to decipher the geology, tectonics, and subsequent evolution of these rocks. In many cases, major element whole rock (WR) analysis yields the first clues about a rock's origin. *Shand* [1927] classified rocks as peraluminous if the whole rock molar ratio of $Al_2O_3/(CaO + Na_2O + K_2O)$ (ASI; Aluminum Saturation Index) is greater than 1. Rocks with ASI < 1 are classified as metaluminous (or subaluminous). This definition is strictly compositional, though later studies attributed variations in WR ASI to the differences in the source material—either sedimentary or igneous—involved in granitoid generation [e.g., *Chappell and White*, 1974, 2001].

Part of the (S)edimentary and (I)gneous granite classification scheme for the Lachlan Fold Belt, southeastern Australia proposed by *Chappell and White* [1974, 2001] defined (S)edimentary-type granites as those with ASI values in excess of 1.1, resulting in saturation of strongly peraluminous phases such as cordierite, garnet, or muscovite [*Chappell and White*, 1974, 2001; *White et al*., 1986a,b; *Miller*, 1985, 1986; *Patiño Douce*, 1992]. In later work, *Chappell et al*. [2012] discussed the origins of ~50% of the Lachlan Fold Belt I-type granites with 1 < ASI < 1.15 [*Chappell*, 1999], which was partially attributed to incongruent melting of biotite and amphibole in the source rocks to form pyroxenes, with incorporation of excess Al into the liquid, thus resulting in peraluminous melts. Other origins for peraluminous rocks include fractional crystallization [*Cawthorn and Brown*, 1976; *Gerdes et al*., 2002; *Chappell et al*., 2012] or loss of volatile alkalis from the magma during cooling [*Zen*, 1986].

While the WR ASI may be attributed to certain processes of felsic rock formation and evolution, the melt ASI may also influence physical properties of melts. Experimental studies demonstrated that Al can exist in

multiple coordination states (e.g., fourfold, fivefold, and sixfold), which is partly a function of the ASI of the melt [*Neuville et al*., 2004; *Mysen and Richet*, 2005; *Mysen and Toplis*, 2007]. The ASI may influence viscosity, where melts or glasses with ASI >1 yielded higher viscosities than those with ASI <1 for the same temperature and SiO_2 content [*Toplis et al*., 1997a, 1997b; *Toplis and Dingwell*, 2004]. Put another way, samples with $\sim$68 wt % SiO_2, and ASI = 1.1 or 0.9 yield the same viscosity ($10^{10.78}$ Pa s) only if the respective temperatures are $\sim$870 and $\sim$750°C [*Toplis et al*., 1997b].

We were motivated to explore whether differences between metaluminous and peraluminous rocks are also reflected in the accessory mineral zircon. Zircon is a particularly interesting target because ages can be determined by U-Pb geochronology and it has the capability of surviving sedimentary cycling which could provide researchers with a tool to probe the ASI of rock samples long since destroyed. We hypothesized that excess moles of Al_2O_3 relative to CaO, Na_2O, and K_2O will result in elevated alumina activities and higher Al concentrations in zircon. To test this, Al in zircon concentrations were measured from 19 geographically and petrogenically diverse rocks with variable ASI. This reveals that zircon derived from peraluminous rocks yield higher average Al concentrations than grains from metaluminous rocks. These data are used to infer metaluminous or peraluminous source rock origins for detrital grains with ages from approximately 3.3 to 4.2 Ga. We specifically target the Jack Hills zircons as they enable us to explore the ASI compositional boundary for silicate rocks in the absence of a preserved rock record; that is, before 4.0 Ga.

2. Samples and Strategy

2.1. Al Substitution in Zircon

Stoichiometric zircon contains tetravalent cations, and therefore, the entry of trivalent Al into zircon requires charge balance. *Trail et al*. [2011] synthesized zircons in the ZrO_2-SiO_2-Al_2O_3-H_2O system and documented a strong correlation between ppm Al and OH concentrations in zircon, where the respective concentrations were determined by electron microprobe and Fourier Transform Infrared Spectroscopy. *Trail et al*. [2011] therefore showed that $^{IV}Al^{3+} + H^{+} \rightarrow {}^{IV}Si^{4+}$ was a viable substitution mechanism, and so water and alumina activity may both determine Al solubility in zircon. The rocks investigated here contain differences in alumina and water activities. Relative differences in alumina/H_2O activities—based on formation environment, mineralogy, and WR chemistry—are considered when possible.

2.2. WR Samples

Zircons are mostly from Lachlan Fold Belt (LFB) samples, southeastern Australia. The LFB contains more than 400 different granitoid plutons, most with ages from 420 to 390 Ma [*White and Chappell*, 1983; *Chappell and Simpson*, 1984]. The geologic and tectonic history of the LFB makes it particularly easy to spatially and chemically investigate the geochemical differences of zircons from chemically diverse parent rocks.

Six peraluminous rocks (ASI >1) were sampled from the LFB, where the Cowra, Cootralantra, Bullenbalong, Dalgety, and Shannons Flat granitoids are plutonic [*Joyce*, 1973; *Hine et al*., 1978; *Chappell et al*., 1990, 1993], and one sample is from the Laidlaw volcanic suite [*Wyborn et al*., 1982]. The samples have a range of ASI values, including those that do not contain a strongly peraluminous phase such as cordierite, muscovite, or garnet. Dalgety and Shannons Flats, for example, have WR ASI values that are weakly peraluminous. In these cases, the excess Al above that required to crystalize feldspars is contained in biotite. While the ideal biotite atomic ratio of Al/(K + Na) is 1, vacancies in the interlayer cation and Tschermak's substitution (i.e., ^{VI}(Mg,Fe)^{IV}Si = ^{VI}Al^{IV}Al) mean this ratio can exceed 1. In other words, biotite in peraluminous rocks can approach the eastonite-siderophyllite join [*Speer*, 1984; *Zen*, 1986].

Six metaluminous rocks (ASI <1) were also sampled. The Tara, Jindabyne, Buckleys Lake, Glenbog, and Moruya plutons [*Griffin et al*., 1978; *Hine et al*., 1978; *Chappell et al*., 1990] are typically classified as I-type rocks [*Chappell and White*, 1974]. The final LFB rock sample with ASI <1 is from the (A)norogenic-type Watergums pluton [*Clemens et al*., 1986]. A-type rocks tend to be higher temperature, water deficient magmas that are possibly derived from partial melting of felsic granulite [*Collins et al*., 1982]. Such samples enable a comparison of Al solubility in zircon from metaluminous rock types with different water activities. A-type rocks are less abundant in southeastern Australia, so high temperature metaluminous plutonic rocks sampled from the Aganenticus, White Mountain, Mt Ascutney, and Pawtuckaway from New England, USA, supplement the LFB suite [*Daly*, 1926; *Shearer*, 1976; *Brooks*, 1990; *Eby et al*., 1992].

Table 1. Samples Collected and Processed for Zircons as Part of This Study

Name	Sample #	Batholith or Complex	Latitude[a]	Longitude[a]	ASI[b]	IUGS Classif.	Classif.
Cootralantra	W058	Berridale	36°16′44.40″S	148°45′25.86″E	1.16	Granodiorite	S
Bullenbalong	W060	Kosziousko	36°18′19.44″S	148°40′6.84″E	1.18	Granodiorite	S
Dalgety	W064	Berridale	36°28′51.48″S	148°50′54.90″E	1.06	Granodiorite	S
Shannons Flat	W074	Murrumbidgee	35°32′17.60″S	148°52′9.90″E	1.03	Granodiorite	S
Laidlaw (volcanic)	W079	Murrumbidgee/Berridale	35°23′ 49.7″S	149°07′20.3″E	1.07	Rhyodacite	S
Cowra	W183	Wyangala	33°49′46.90″S	148°41′41.10″E	1.27	Granodiorite	S
Tara	W059	Berridale	36°13′47.82″S	148°40′14.88″E	0.98	Granodiorite	I
Jindabyne	W061	Kosziousko	36°26′3.18″S	148°37′43.86″E	0.98	Tonalite	I
Buckleys Lake	W066	Berridale	36°32′48.06″S	149° 2′1.62″E	0.99	Monzogranite	I
Glenbog	W067	Bega	36°36′48.54″S	149°21′53.94″E	0.94	Granodiorite	I
Moruya	W120	Moruya	35°54′15.0″S	150°06′49.1″E	0.90	Tonalite	I
Watergums	W071	Gabo Island	37°17′43.50″S	149°50′14.46″E	0.98	Granite	A
Pawtuckaway	W143	Pawtuckaway	43°6′11.80″N	71°10′50.30″W	0.88	Monzonite	A
Agamenticus	W147	Aganenticus	43°12′18.90″N	70°38′39.90″W	0.98	Granite	A
Conway granite	W162	White Mountain	44°3′47.50″N	71°4′24.50″W	0.96	Granite	A
Mt Ascutney	W173	Ascutney	43°26′9.20″N	72°25′5.50″W	0.96	Granite	A

[a]Datum = WGS84.
[b]Defined in text. Whole rock major element chemistry can be found in supporting information Table S1.

The sample suite also includes zircons from three peraluminous Arunachal leucogranites from the eastern Himalaya. These have WR ASI values of 1.08 and 1.60 [see *Harrison and Wielicki* [2016] and supporting information Table S1 for additional information) but have some key differences when compared to peraluminous samples of the LFB. For instance, LFB granitoids with higher ASI values such as Cowra are cordierite saturated, while Himalayan leucogranites yield muscovite as the primary carrier of excess moles of Al. Arunachal leucogranite zircons yield low crystallization temperatures centered at 660°C [*Harrison and Wielicki*, 2016], similar to low temperatures reported elsewhere for Himalayan leucogranites [*Kohn*, 2014, 2016]. Igneous crystallization of zircon at these temperatures implies minimum melting conditions and a water activity close to or equal to unity. Additional information for the 16 collected WR samples can be found in Table 1 and in the supporting information. The WR data and sample information for the three Arunachal leucogranites can be found in *Harrison and Wielicki* [2016]. Last, detrital zircon samples were collected from the Jack Hills (JH) metaconglomerate discovery outcrop for pre-4.0 Ga zircons as previously reported [e.g., *Compston and Pidgeon*, 1986; *Weiss et al*., 2015].

Table 1 identifies samples as (S)edimentary-type, (I)gneous-type, and (A)norogenic-type rocks [*Chappell and White*, 1974, 2001; *Collins et al*., 1982]. While useful, there are exceptions to this classification scheme, even among the limited sample suite presented here. For instance, the Dalgety and Shannons Flats both have WR ASI values less than 1.1, yet these samples remain classified as S types [*Chappell et al*., 1990]. Here the term "peraluminous" is used for any rock with ASI $>$ 1. The terms "metaluminous I type" and "metaluminous A type" distinguish the two groups of metaluminous samples. Namely, metaluminous A-type rocks are water deficient, and expectedly, yield higher zircon crystallization temperatures than metaluminous I types. Peralkaline rocks were not sampled (i.e., Na + K $>$ Al). The WR ASI values are utilized throughout this paper as a point of reference. However, granitoids may contain a significant component of crystals that did not crystalize from the melt. These crystals may represent parts of the source rock, or alternatively, crystals from the source rock that underwent recrystallization during cooling [*Chappell et al*., 1987].

3. Methods

Zircons were processed from hand samples by typical crushing and heavy mineral separation techniques, but additional steps were needed before grain mounting because radiation-damaged zircons are known to contain secondary Al. For instance, *Medenbach* [1976] conducted trace element analyses of zircons of variable structural integrity from diverse localities and found that some zircons yielded high Al contents. These high Al contents, which in many cases were detected at weight percent levels, are also *strongly* correlated with high Ca and Fe concentrations in electron microprobe spot analyses and element maps. To our knowledge, the *Medenbach* [1976] work is the first mention of such high apparent Al concentrations in zircon. Reconnaissance ion microprobe analyses of untreated Jack Hills zircons also revealed apparent Al concentrations as high as 200 ppm, which were not considered to be robust lattice measurements.

Thus, all zircon-bearing heavy mineral separates (Table 1) and Jack Hills grains were soaked and sonicated in cold hydrofluoric acid (HF) for ~10 min to remove radiation-damaged zircons or regions. Grains were then mounted, cast in epoxy, and polished to 1 μm with SiC or diamond. The surfaces of all sectioned grains were cleaned in HF for a few minutes before analysis as an additional precaution. Cathodoluminescence (CL) images were collected to guide analytical spot locations.

3.1. LA-ICP-MS Spot Mode for Zircons of Known Provenance

Lachlan Fold Belt and New England (USA) zircon samples were analyzed with a Photon Machines 193 nm G2 laser ablation (LA) system equipped with a HelEx 2-volume sample chamber connected to an Agilent 7900 inductively couple plasma mass spectrometer (ICP-MS) quadrupole at the University of Rochester, or using the LA-ICP-MS Photon Machines Analyte connected to Varian 820-MS quadrupole at Rensselaer Polytechnic Institute. Zircon crystals from Cowra, Cootralantra, Bullenbalong, Dalgety, and Shannons Flat rocks are known or suspected to contain restitic cores that did not completely dissolve during granite genesis and therefore do not represent the chemistry of the magma [*Gulson and Rankin*, 1977; *Williams et al*., 1992]. The rims of crystals were targeted, guided by CL images.

Grains were carefully screened for inclusions with transmitted and reflected light microscopy. Spot locations were chosen by identifying crystal regions visibly free of inclusions. Locations were also cross-checked with CL images before ablation. We further utilized the reflected light (to focus on the zircon surface) and transmitted light (to check for subsurface inclusions) features on the Photon Machines LA camera unit. A laser fluence of 4.9–7 J/cm^2 with pulse rate of 10 Hz was used for 20 s of total ablation time. The HelEx 2-volume sample chamber had flow rates set to 0.6 L/min for He flow within the sample chamber (MFC1). The He flow in the HelEx arm was set to 0.2 L/min (MFC2).

Zircons were ablated with a spot size ranging from 10 to 35 μm. Typical masses included ^{7}Li, ^{23}Na, ^{24}Mg, ^{27}Al, ^{29}Si, ^{39}K, ^{44}Ca, ^{49}Ti, and ^{57}Fe, though ^{7}Li and ^{49}Ti were not always analyzed. Initially, Li was quantified to explore the relationship between the zircon Al/Li and the the whole rock ASI. The elements K, Na, Mg, Ca, and Fe were analyzed because they are not expected to be structurally accommodated by the zircon lattice in appreciable quantities. Therefore, these elements are used to screen the laser ablation signal for inclusions or metamict grain regions not removed during the HF cleaning step.

Muscovite has low K/Al, which can make it a challenging inclusion to identify during ablation. Introducing He into the collision cell of the Agilent 7900 ICP-MS increased counts of K relative to Al. A He gas flow of ~1 mL/min was used based on trial-and-error analyses of muscovite, to obtain counts of K that were at least a factor of 3 greater than Al, a strategy used to explore for the possibility of microinclusions of muscovite in strongly peraluminous samples. Similar tests were also conducted for cordierite.

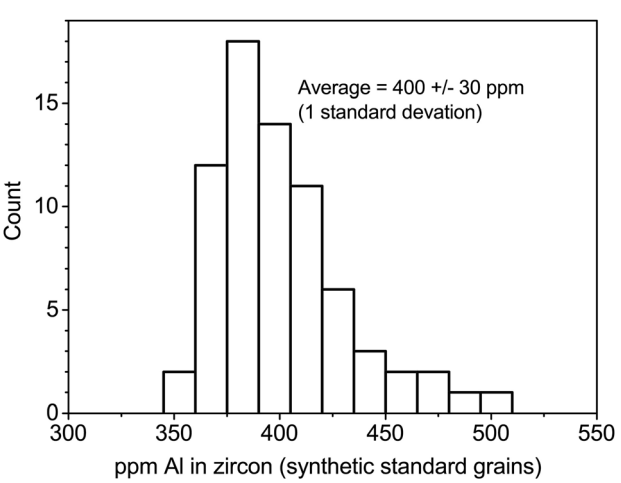

Figure 1. LA-ICP-MS and ion microprobe analysis utilized zircons from this standard aliquot. The absolute concentrations were determined by electron microprobe (n = 72).

The ICP-MS signals were carefully evaluated with the Iolite 3.x software package [*Paton et al*., 2010, 2011]. "Spikes" of contaminant elements K, Na, Mg, Ca, and Fe often occurred with spikes of Al contents, and were excluded from the final results (see supporting information figure). While K, Na, Mg, Ca, and Fe may be incorporated into the zircon lattice in trace quantities, we erred on the side of caution and excluded block data in which these elements were detected. Uniformly high counts of K, Na, Mg, Ca, or Fe resulted in complete exclusion of approximately 5% of the zircons analyzed.

Silicon-29 was used as an internal standard and Al in zircon concentrations were standardized against NIST612 glass

[*Pearce et al.*, 1997] or synthetic Al-doped zircons produced after the technique described in *Trail et al.* [2011]. The Al concentrations of several synthetic zircons were determined using the Cameca sx100 electron microprobe at Rensselaer Polytechnic Institute, yielding an average value of 401 ± 30 ppm Al (Figure 1). Synthetic zircons were standardized against NIST612 for LA-ICP-MS work, which enables a comparison of matrix-related fractionation of elements (Al from Si) as a function of spot size. No observable matrix effects were detected for spots 20 μm or larger; that is, calculated Al in zircon concentrations were comparable to electron microprobe results. However, apparent Al concentrations in zircon deviated by up to 40% from the true value for spot sizes <20 μm. Unknowns analyzed with spot sizes <20 μm utilized synthetic zircon standards exclusively.

3.2. Secondary Ion Mass Spectrometry Analyses for Zircons of Known Provenance

Secondary ion mass spectrometry (SIMS) analyses were undertaken using the UCLA CAMECA *ims*1270 for zircons from the Arunachal leucogranites. Epoxy mounts were ultrasonically cleaned in a sequence of soapy water, deionized water, and methanol, and then Au coated. For each analysis, we collected $^{23}Na^{+}$, $^{27}Al^{+}$, and $^{30}Si^{+}$ using the axial ETP electron multiplier through peak switching with a mass resolving power of ~4000 which is sufficient to resolve all relevant molecular interferences. Al concentrations were calculated relative to the synthetic zircon standard (see section 2.1 and Figure 1). A primary beam intensity of 10 nA with a spot size of ~25 μm was used in each analysis. In order to remove any surface contamination, the primary beam was rastered over the sample prior to each analysis using a 20 μm raster size for 3 min. The SIMS data were examined in a similar manner to the LA-ICP-MS data (section 2.2) to search for evidence of inclusions. We did not find any evidence for spikes in Al concentration and instead found uniform Al^{+} intensity once we removed any surface contamination. These findings suggest that high Al content is not due to small inclusions but is structurally bound in the zircon.

3.3. LA-ICP-MS Spot Mode for Archean and Hadean Detrital Zircons

Two types of analyses were conducted. In the first case, U-Pb ages and trace element chemistry of 50 grains were determined simultaneously using a 30 μm spot, with one to three analyses for each grain. The mass table consisted of ^{7}Li, ^{23}Na, ^{24}Mg, ^{27}Al, ^{29}Si, ^{44}Ca, ^{52}Cr, ^{57}Fe, ^{49}Ti, ^{202}Hg, ^{204}Pb, ^{206}Pb, ^{207}Pb, ^{235}U, and ^{238}U, and resulted in a limit of detection of ~2–3 ppm for Al. This detection limit was low enough to establish whether the zircons were more likely derived from peraluminous versus metaluminous samples. Ages were standardized against AS-3 zircon [*Paces and Miller*, 1993], and a secondary in-house zircon standard from the same locality as the 91500 zircon [*Wiedenbeck et al.*, 2004; *Trail et al.*, 2015]. Once it was established that most JH zircons yielded below 2–3 ppm of Al, the analytical strategy was modified for the subsequent 225 grains to lower the detection limit for Al. First, the U-Pb ages were determined using a 25 μm spot size and the following mass table: ^{202}Hg, ^{204}Pb, ^{206}Pb, ^{207}Pb, ^{235}U, ^{232}Th, and ^{238}U. Second, a 35 μm spot was placed directly next to the age spot in the same CL zone with the following masses analyzed: ^{7}Li, ^{23}Na, ^{24}Mg, ^{39}K, ^{27}Al, ^{29}Si, ^{44}Ca, ^{57}Fe, and ^{49}Ti. This yielded a detection limit of ~0.2 ppm for Al.

3.4. Depth Profiling by LA-ICP-MS

Several crystals from four separate zircon aliquots—peraluminous volcanic (Laidlaw), peraluminous plutonic (Dalgety), metaluminous A-type plutonic (Watergums), and metaluminous I-type plutonic (Jindabyne)—were depth profiled by LA-ICP-MS. All crystals were cast in the same epoxy mount, very gently polished in colloidal silica for 2 min, and then sonicated to eliminate surface contamination. Zircons were ablated from their rims into their interior for 20 s with a mass table of ^{23}Na, ^{24}Mg, ^{27}Al, ^{29}Si, ^{39}K, ^{44}Ca, and ^{57}Fe. The data were discretized in ~1 s blocks. If inclusions were encountered, this portion of the depth profile was excluded from further consideration. Synthetic zircons containing ~400, 100, and 40 ppm Al were also ablated and Al/Si was monitored versus depth to check for instrument-related elemental fractionation. "Laser on" time was converted to depth by removing select grains from epoxy, rotating 90°, remounting, and then polishing to expose the laser pit in cross section. This revealed that 1 s of ablation translates to a little over a micron of removed material. Cathodoluminescence imaging was conducted afterward to characterize the internal zoning of the crystals. The supporting information contains additional information about the details of grain manipulation.

4. Zircons of Known Provenance: Results and Discussion

Representative CL images and analytical locations are found in Figure 2. The LA-ICP-MS and SIMS analyses of zircons of known provenance reveal a clear relationship between Al in zircon concentration and whether

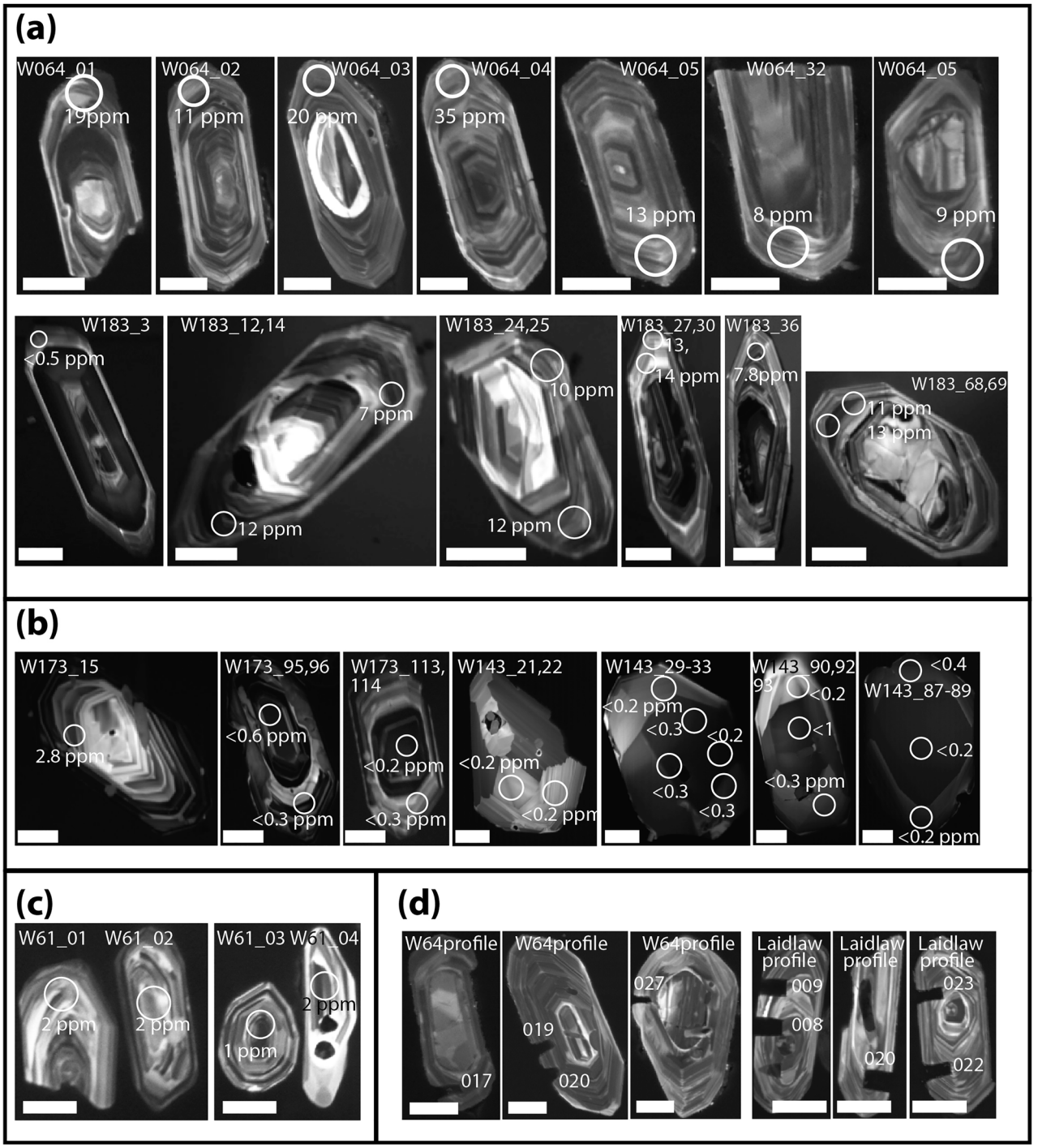

Figure 2. Representative CL images of zircons used for exploring Al in zircon concentrations from known rock types. Analytical locations are labeled with either (a–c) Al content in ppm or (d) profile number. All scale bars are 50 μm. (a) Peraluminous zircons from Dalgety (W64) and Cowra (W183). These zircons typically contain restitic cores the rims of these crystals were targeted, and others like them. (b) High temperature metaluminous A-type samples from Mt Ascutney (W173) and Agamenticus (W143). (c) Metaluminous I-type zircons from the Jindabyne tonalite. (d) Depth profiled zircons, rotated orthogonal to the ablation direction, and polished to expose the ablation pits in cross section. Some pits penetrate to inherited cores.

WR ASI is greater or less than unity (Figure 3). Strictly, ASI values are a measure of charge balance with feldspar stoichiometry [*Shand*, 1927], and therefore could be corrected for the removal of Ca associated with apatite. Here ASI values are not corrected for apatite. Zircons from metaluminous granitoids with higher temperature affinity (i.e., A-type samples) yield, on average, the lowest recorded Al concentrations, with average values of <1 ppm ($n = 259$). Zircons from lower temperature metaluminous granitoids (I types) are

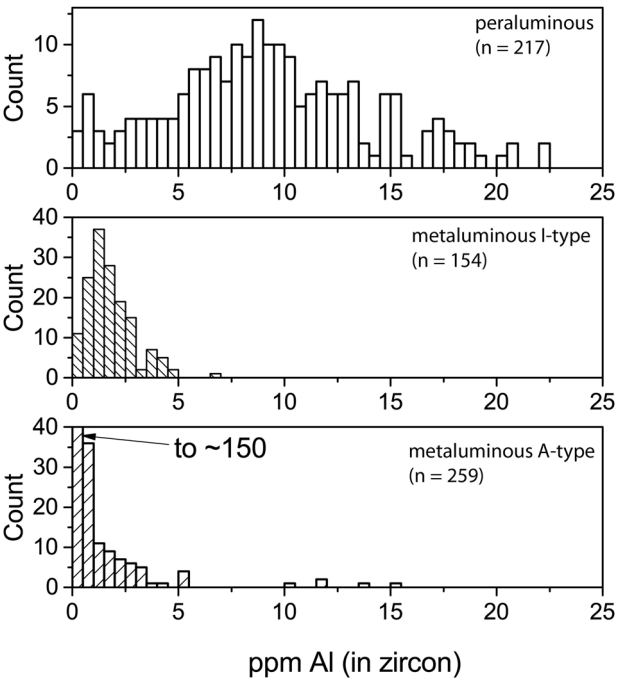

Figure 3. The Al in zircon contents (in ppm) from peraluminous rocks show resolvable differences when compared to metaluminous I-type and high temperature metaluminous A-type samples. Approximately 5% of the Al concentrations from peraluminous zircons plot at values that range from 25 ppm to approximately 35 ppm, with one datum at 74 ppm (not shown).

slightly higher, with average Al contents of ~2 ppm (n = 154). In both cases, >90% of the concentrations fall within 2 ppm of the average. In contrast, Al contents of zircons found in peraluminous rocks reflect a broadly normal distribution centered at ~10 ppm (n = 217) in which ~30% of the data fall within 2 ppm of the average.

There is a step function-like increase in Al in zircon concentration when ASI of the WR exceeds one (Figure 4). Notably, the high Al contents observed in zircons from peraluminous rocks are not exclusively linked to the saturation of a strongly peraluminous phase such as cordierite, garnet, or muscovite. For example, Dalgety and Shannons Flats (ASI = 1.06 and 1.03, respectively) have broadly similar Al in zircon concentrations when compared to rock samples with a strongly peraluminous minerals, such as Cowra (cordierite saturated). Here an Al in zircon concentration of 4 ppm value is considered to separate peraluminous from metaluminous samples. Examination of the I/A-type zircon data reveal that 95% of the results contain Al concentrations ≤4 ppm. By comparison, about 15% of the zircons from peraluminous rocks contain Al contents ≤4 ppm.

The heterogeneous distribution of Al contents in zircon for the peraluminous samples may have important implications for magma evolution. We rule out analysis of restitic cores as completely responsible for this variation, though we recognize the limitations involved in precisely defining the overgrowth-restitic core boundary based on CL pattern recognition alone (e.g., Figure 1). Instead, we hypothesized that the range in recorded Al concentrations for peraluminous zircons may reflect evolution of the alumina activity (and/or water activity) of the system during zircon crystallization.

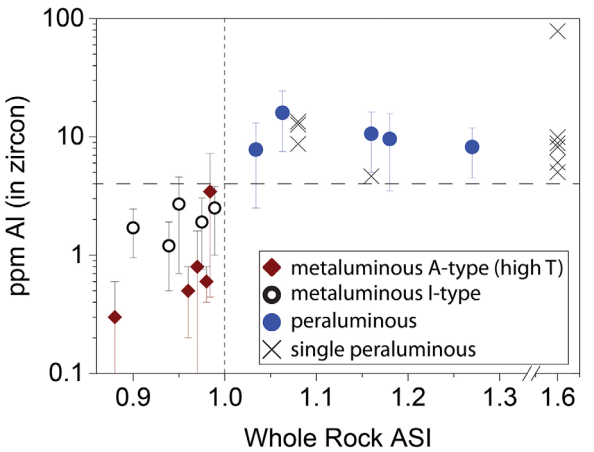

Figure 4. Lognormal plot of Al in zircon concentrations versus whole rock ASI; for samples with less than 10 analyses, individual analyses are represented by "cross." Zircons from rocks with ASI > 1 yield distinctly higher Al concentrations than zircons from rocks with ASI < 1. Metaluminous high T samples (A type) typically yield zircons with Al contents <1 ppm. No peralkaline rocks were investigated in this study. The horizontal dashed line (at 4 ppm) separates peraluminous from metaluminous zircons.

This hypothesis cannot be explored with algorithms such as Rhyolite-MELTS [*Gualda et al.*, 2012] because thermodynamic data for peraluminous rocks are sparse or altogether absent. Furthermore, the WR values do not represent chemical composition of the melt, and granitoids may contain crystals that did not crystalize from the melt. For example, peraluminous (S-type) samples contain cordierite, sillimanite, and garnet, and metaluminous I-types are dominated by plagioclase crystals and pyroxenes, which are derived from the source rocks [*Chappell et al.*, 1987]. It is also true that Figure 4 does not accurately capture the

complexities of alumina activity evolution of the system between initial zircon saturation, and final zircon growth.

As an alternative to modeling or exclusive reliance on WR ASI values, depth profile experiments were conducted to explore relative changes in alumina activity and/or water activity—see section 2.1—by quantifying Al concentrations versus depth for four sample suites (Figure 5a). For reference, average Al concentration versus depth for three different aliquots of synthetic Al-doped zircons (~400, 100, and 40 ppm) exhibit no resolvable change in Al concentration with depth (Figure 5b). In other words, there is no instrumental fractionation of Al from Si as a function of pit depth. Zircons from the metaluminous Jindabyne sample exhibit little to no change in Al concentration with depth, and Watergums A-type zircons show, on average, a subtle increase in Al concentration with depth to maximum values of ~4 ppm (Figures 5c and 5d). Average Al concentration trends in peraluminous samples broadly decrease with depth; CL images for data presented in Figures 5e and 5f can be found in Figure 2.

Some Laidlaw zircons show evidence—in CL images—that depth profiles intersect restitic cores (Figure 2). These images are used to annotate Al in zircon concentration versus depth data with arrows to show the

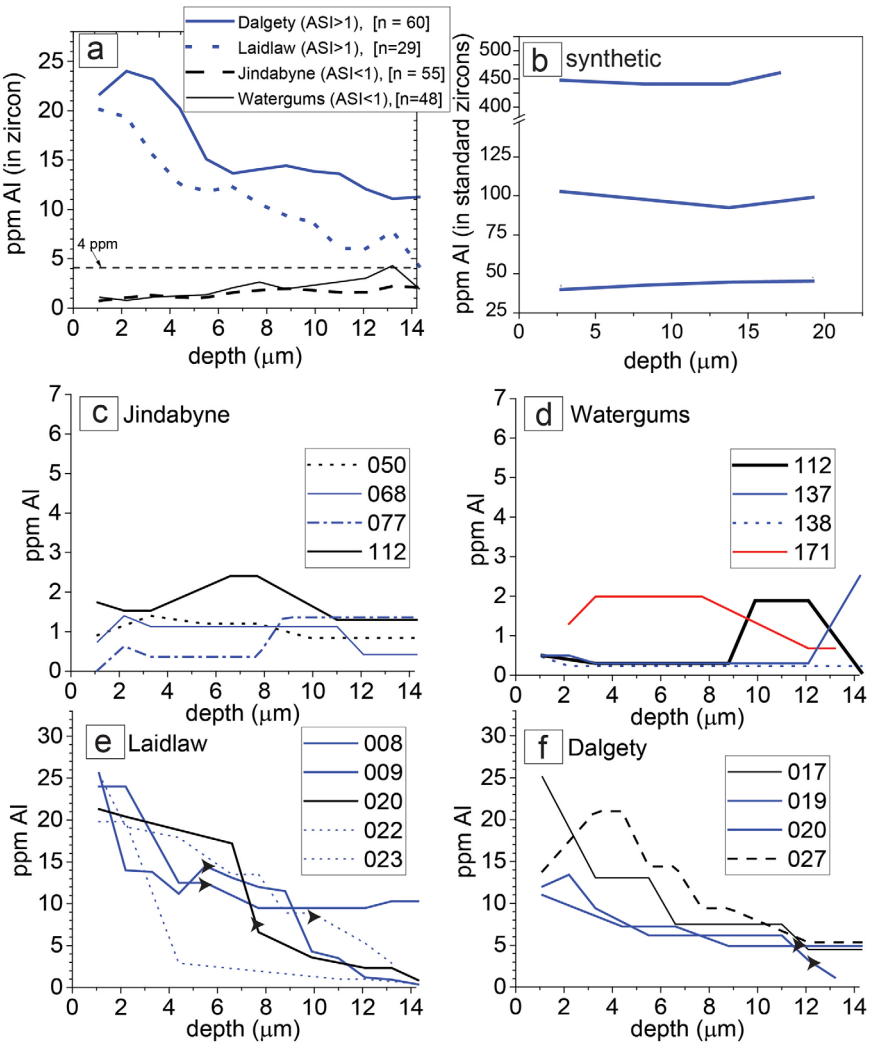

Figure 5. Al concentrations from the rim to the interior domains determined by LA-ICP-MS depth profiles. (a) The lines reflect the averages for all zircons analyzed for each of the four samples (individual analyses can be found in the supporting information Table S2). Al concentrations trend toward subtly higher values in the interiors of metaluminous crystals, in contrast to peraluminous zircons. (b) No instrumental fractionation of Al from Si is observed for zircon standards; i.e., Al concentration versus depth remains constant. (c, d) Al concentration remains broadly constant versus depth for individual metaluminous samples; note that the numbers correspond to the CL numbers provided in Figure 2. (d, e). Al concentration decreases versus depth for individual peraluminous zircon samples. Arrowheads indicate the probable depth where the restitic cores are intersected, if applicable.

approximate location of probable restitic core intersection. Data collected after this interval are not likely to be related to the melt generated for this peraluminous sample. The same exercise was conducted for the Dalgety zircons. In some cases, depth profiles were far enough away from the central regions of the crystals that no obvious restitic cores are encountered (e.g., CL image *W64profile_17* in Figure 2). Importantly, the Al contents in these zircons vary with depth, even if the relic core data are omitted.

Most analytical artifacts are ruled out for the observed trends. Surface contamination, for example, is ruled out for several reasons. First, all zircons were treated in HF acid which should remove any possible silicate contaminant still attached to the surface of the zircon crystals. Second, grains were gently polished with colloidal silica before analysis as an additional precaution. Third, all grains were mounted in the same mount, and therefore any surface contamination should affect all grains. The latter is important because the Al concentrations of the surfaces of A-type Watergums and I-type Jindabyne zircons are comparable to spot mode data, which indicates that surface contamination, if present at all, is negligible.

Other analytical artifacts that could affect depth profiles include the washout times of the ablation cell. For A-type and I-type zircons, the concentration change from rim to interior domain is small enough (a few ppm) that it is of little concern, but it could be important for peraluminous zircons. Tests on Al in zircon standards show that Al counts decrease by an order of magnitude in 1 s for the HelEx cell. For this reason, and because there may be some progressive contamination of deeper parts of the profile from the walls of the ablation pit, the actual change in Al concentration versus depth is likely slightly greater than the data indicates.

Nevertheless, these data further support the idea that (1) higher alumina activity environments of peraluminous melts are reflected in Al in zircon concentrations and (2) peraluminous melts can exhibit measureable changes in alumina activity over the temperature range of zircon crystallization. Both topics are addressed in the next two sections.

5. Alumina Activity of Metaluminous and Peraluminous Melts

Although peraluminous and metaluminous rocks have comparable WR Al concentrations, Al in zircon concentrations from peraluminous rocks are about a factor of 5 higher than grains from metaluminous rocks. To explain this difference, the structural role of Al in a melt is considered, accepting that there is some general relationship between the composition of the WR and the melt from which the zircon grew. In silicate melts, it is generally assumed that Al is a principal network-forming cation. This is so because Al is tetrahedrally coordinated in association with low-field-strength cations such as Na^+ and K^+ to satisfy charge balance with Al^{3+} [*Mysen and Richet*, 2005; *Mysen and Toplis*, 2007]. Charge balance may also be satisfied with Ca^{2+}. This requires Ca association with two AlO_4 tetrahedra for charge compensation [e.g., *Mysen et al*., 1981].

For ASI $>$ 1, some Al ions lack the necessary change compensating cations, and so the proportion of Al that can exist in fivefold and even sixfold coordination increases [*Neuville et al*., 2004]. Alternatively, Al not associated with a charge balancing cation may form Al triclusters—in fourfold coordination—that contribute to the polymerization of the melt [*Mysen and Toplis*, 2007]. If SiO_2 is held constant, maximum viscosities of silicate melts often exist in the peraluminous field, supporting this model [*Riebling*, 1966; *Le Losq et al*., 2014; *Toplis et al*., 1997a,b]. In both scenarios discussed above, the structural role of some of the Al in peraluminous melts does not depend on association with K, Na, or Ca. These Al atoms could result in elevated alumina activity in the melt, which could explain why zircons derived from peraluminous melts yield higher Al concentrations.

Higher Al concentrations in minerals from peraluminous rocks is not restricted to zircon. For instance, Al/(Na + K) values in biotite are higher in peraluminous rocks when compared to metaluminous samples [e.g., *Zen*, 1986; *Chappell et al*., 2012] and Al contents in quartz from peraluminous rocks are broadly higher than quartz from metaluminous samples [*Breiter et al*., 2013; *Ackerson et al*., 2015].

6. Changes in Alumina Activity During Magma Evolution

The data show that there is some relationship between the alumina activity of a silicic melt and ASI of the whole rock—even if it is not a simple one—in agreement with conclusions reached by others [e.g.,

Miller, 1985; *Patiño Douce*, 1992; *Acosta-Vigil* et al., 2003]. For example, the average Al in zircon concentrations for peraluminous rocks are broadly similar and appear to be independent for ASI > 1. Changes in the alumina activity of peraluminous melts along the liquid line of descent are probable because depth profile data show variable uptake of Al in zircon.

We review some key topics that could influence the alumina activity of peraluminous melts. To start, we consider variables that establish the ASI of a melt during generation from the source rock. Of particular relevance is an experimental study conducted by *Acosta-Vigil et al*. [2003] in which alumina solubility in granitic melts was investigated primarily as a function of T and water activity. These authors showed that the progressive addition of water to their experimental samples resulted in additional dissolution of strongly peraluminous phases, such as muscovite, corundum, and aluminosilicates. This was reinforced in a study *London et al*. [2012] that involved juxtaposing a haplogranite with a metapelite to explore anataxis/assimilation. A positive correlation between ASI and H_2O was also observed in earlier experimental studies by *Clemens and Wall* [1981] and *Dingwell et al*. [1997]. *Acosta-Vigil et al*. [2003] proposed that H^+ may serve a role similar to low-field-strength cations such as Na^+ and K^+ to satisfy charge balance with Al^{3+} in fourfold coordination. If so, then part of the decoupling of ASI from alumina activity depends on the H_2O activity of the melt. In this study, increasing temperature from 700 to 800°C resulted in additional dissolution of peraluminous phases and therefore melts with higher ASI values.

Thus, ASI values of anatectic melts are at least a function of T, water activity, and the source rock. We now consider monotonic cooling of an anatectic peraluminous melt in a closed system (i.e., no mass transfer) although this clearly oversimplifies granitic magma evolution. In experiments that mimic a closed system, glass compositions from 880 to 710°C (2–5 kbar) show that the change in ASI of the melt—and perhaps alumina activity—is not monotonic, but instead oscillates [e.g., *Puziewicz and Johannes*, 1988]. Feldspar crystallization from a peraluminous melt along the liquid line of descent will increase ASI of the residual melt, but perhaps only up to a point. For instance, a melt with ASI > 1.2 could instead be driven to lower ASI values by the saturation of an alumina activity buffering phase such as andalusite [*Chappell*, 1999], as a result of the low solubility of strongly peraluminous phases at lower temperatures.

However, most granitic melts are not closed systems, and it is perhaps more interesting and certainly more relevant to consider what happens in an open system. Loss of Na and/or K to the vapor phase during cooling [e.g., *Zen*, 1986; *Chappell*, 1999] would likely lead to an increase in the alumina activity of the remaining system. If water (H^+) is involved in the fourfold coordination of Al in the melt, its loss could also cause the remaining system to evolve to higher alumina activities. In contrast, removal of strongly peraluminous phases from the system via fractional crystallization or by eruption [*Morgan et al*., 1998] would likely lead to a decrease in the alumina activity. Peraluminous melts generated by partial melting of sedimentary rocks may also become progressively more peraluminous by fractional crystallization of feldspar, as is suspected to occur in the LFB [*Chappell et al*., 1998; *Chappell*, 1999].

An increase in alumina activity of the system along the liquid line of descent may explain why depth profiled zircons from peraluminous rock samples yield, on average, higher Al concentrations on the rims than the interior domains. However, this simple interpretation is complicated by the need for Al charge balance in zircon. Since Al can enter into the zircon lattice with H^+ (section 2.1) water activity plays a role in the solubility of Al in zircon.

To first order, however, water activity probably does not drastically affect Al solubility in zircon. For instance, the Himalayan Arunachal leucogranite zircons have Ti-in-zircon crystallization temperatures with a dominant peak at 660°C, consistent with fluid present conditions [*Harrison and Wielicki*, 2016]. Peraluminous LFB zircons have higher average zircon crystallization temperatures of ~730°C suggesting crystallization at lower water activity. Despite these differences, the recorded Al concentration among these sample suites is similar. Moreover, water deficient A-type samples crystalize zircon at ~790°C with lower Al concentration (~1 ppm) than the lower temperature (~740°C) I-type counterparts (~2 ppm Al). This ~1 ppm difference is small since the average Al concentration from peraluminous samples is ~10 ppm.

And finally, zircons within the same peraluminous rock may experience different alumina activity evolution paths. Depth profiles for a few peraluminous zircons yielded rim Al concentrations in the 2–4 ppm range in <5% of the analyses (e.g., Laidlaw 012SMPL.d or Dalgety 010SMPL.d in supporting information Table 2), which is well below the average rim concentration of ~20 ppm. Zircons have been found as inclusions

within major phases, such as biotite in LFB peraluminous rocks [*Hine et al*., 1978; *Phillips et al*., 1981; *Healy et al*., 2004], and biotite-rich xenoliths that are metasedimentary in origin are documented [*Joyce*, 1973]. If the zircon remains in encapsulated within biotite from the restite, for example, this chemical isolation would explain the lower Al concentrations observed.

7. Al Contents in Archean and Hadean Detrital Zircons

The quantification of Al contents in detrital zircons represents a compelling opportunity to investigate the relative abundance of peraluminous-derived versus metaluminous-derived zircons preserved in the sedimentary record. Exploring the chemical composition and nature of early terrestrial magmatism and rock recycling is essential if we are to understand the dynamics of our planet, propose chemical constraints for the evolution of the Earth, and define the chemical makeup of weathered material that may have played a role as a substrate for the origin of life.

We reiterate that 95% of the metaluminous data yield concentrations less than 4 ppm, although upward of 15% of peraluminous zircons collected in spot mode have Al contents <4 ppm. This percentage diminishes to $<5\%$ if only the depth profile samples are considered. For Hadean zircons, only spot mode analyses were conducted (Figure 6). This avoids conflating issues with the analysis of younger overgrowths in Archean and Hadean zircons [e.g., *Trail et al*., 2007]. Given these two pieces of information, we estimate that detrital zircons with 4 ppm Al or greater are likely derived from peraluminous melts. If the data from known source rocks is used as a guide, this concentration threshold will result in an underestimation of the total number zircons derived from peraluminous samples perhaps by $\sim$10% (also taking into consideration that 5% of metaluminous samples yield Al concentrations that exceed 4 ppm).

With these caveats noted, we present the results of Al in zircon concentrations from 275 detrital grains from the Jack Hills with ages that range from 4.24 to 3.29 Ga (Figure 7). If 3290–3775 Ma zircons are considered, then approximately 8% of the grains yield Al concentrations that exceed 4 ppm, suggestive of origins in peraluminous melts. Zircons older than 3.9 Ga ($n = 39$) yield a single occurrence with an Al content that exceeded an average value of 4 ppm. Four analyses produced Al concentrations of 6.2, 4.5, 4.1, and 2.5 ppm. Results from this 4.04 Ga grain are consistent with the presence of peraluminous magmas during the Hadean determined by the presence of muscovite inclusions [e.g., *Hopkins et al*., 2008; *Harrison and Wielicki*,

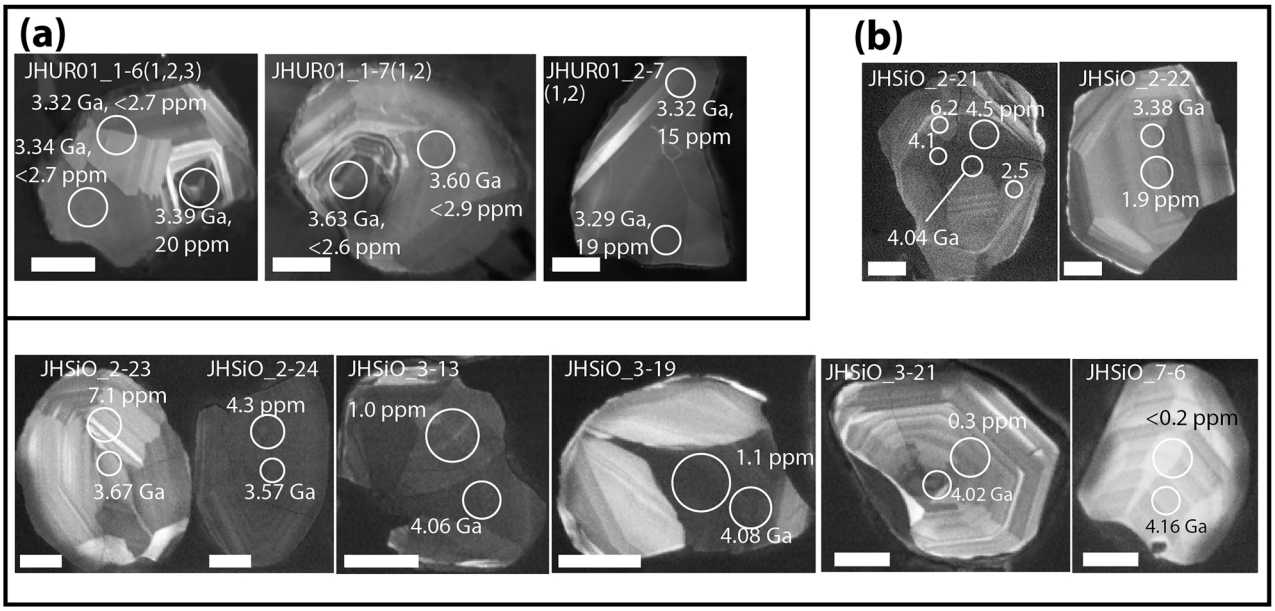

Figure 6. Representative CL images from detrital Archean/Hadean zircons analyzed in this study. (a) Zircons with simultaneous age and Al content measurements (single spot); Al detection limit is 2–3 ppm. (b) Zircons with separate measurements of age and Al content (double spot); Al detection limit is 0.2–0.3 ppm.

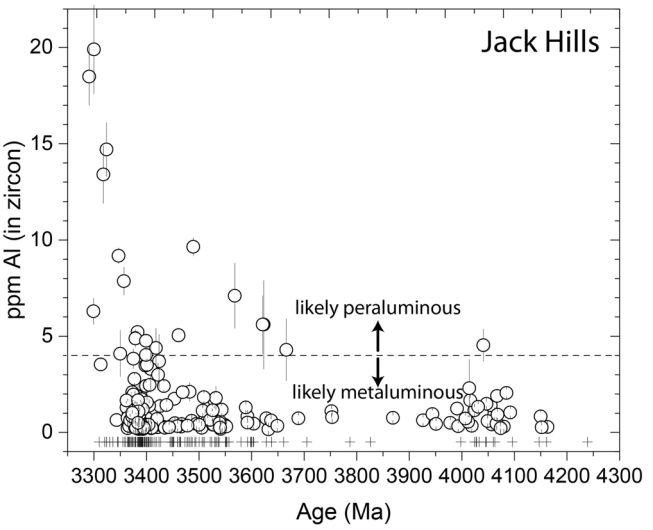

Figure 7. Al concentrations in Jack Hills zircon versus age showing several candidate grains in the detrital population that are likely derived from peraluminous rocks. Analyses with Al concentrations below the limits of detection are plotted as "plus." All data are tabulated in the supporting information tables.

2016]. It is also true that these concentrations, on average, overlap with the highest (upper 5%) concentrations reported for the metaluminous samples. Therefore, this indicator of peraluminous melts is not as robust as demonstrably primary peraluminous mineral inclusions. Nevertheless, the data do show that Hadean zircons (n = 39) are dominantly derived from metaluminous rocks. In a small fraction (~4%) of the samples investigated, Ti-in-zircon crystallization temperatures [*Ferry and Watson*, 2007] and Al contents broadly similar to the high temperature metaluminous (A-type) zircons investigated here.

Some $\delta^{18}O$ values recorded in Hadean zircons provide evidence for low temperature water-rock interaction [e.g., *Valley et al*., 2005], even though there is still considerable uncertainty regarding the chemical composition of the recycled material. Even broad constraints that bear on the nature of recycled material (clays) could help constrain the environments of early Earth, which may be important for certain origin of life models. In some cases, RNA molecules can bind efficiently to certain clays resulting in the formation of longer oligomers, while clays do not exhibit useful bonding properties [e.g., *Ferris and Ertem*, 1993]. The ultimate composition of the weathered Hadean material remains mostly obscured, though evidence for assimilation of large volumes of strongly peraluminous material into Hadean magmas is sparse among the data presented here. Future studies that combine Al concentrations with $^{18}O/^{16}O$ measurements may lead to new insights.

The higher frequency of peraluminous-derived grains from the 3290–3775 Ma age group may reflect a temporal change in the chemical composition or volume of assimilated peraluminous material, or alternatively, by a detrital sample bias. In the case of the latter, 8 of 13 zircons with U-Pb ages between 3300 and 3350 Ma yield Al contents that are consistent with a peraluminous origin, possibly indicating that many of these grains weathered from the same terrain. High abundances of elevated Al concentrations in zircons over discrete time intervals from the detrital record may reflect past orogenic events, given that peraluminous granitoids are common in collisional tectonic settings.

8. Concluding Remarks and Outlook

An important compositional boundary of silicate magmas is defined by whether the molar ratio of $Al_2O_3/(CaO + Na_2O + K_2O)$ is larger or smaller than one. Data show that Al in zircon concentrations are a useful proxy for this melt and WR parameter. Al contents in zircon may also be useful to explore the chemical character of sources involved in granitoid genesis. For instance, *Chappell et al*. [2012] notes that "S-type" rocks within the LFB always contain ASI values greater than 1. On the other hand, many I-type rocks yield ASI > 1, and fractional crystallization may drive melts into the peraluminous field. Granitoid rocks from the Moonbi Suite of the New England Batholith (Australia), for example, show variations from just above ASI values of 0.9 and 65% SiO_2, to ASI values approaching 1.05 and ~75% SiO_2. Others have also shown that peraluminous melts can develop though felsic differentiation (removal of hornblende) of calc-alkaline rocks [*Cawthorn and Brown*, 1976]. In cases where zircon is present, Al contents may trace the evolution of alumina activity during assimilation, fractionation, and crystallization. Finally, many of the models of magma evolution are conceptual, qualitative, and oversimplified scenarios. In this regard, experiments are needed in order to understand the relationship between ASI, alumina/H_2O activity, and Al in zircon concentrations more rigorously.

Acknowledgments
This work was supported by NSF grant EAR-1447404 to D. Trail. The ion microprobe facility at UCLA is partially supported by a grant from the Instrumentation and Facilities Program, Division of Earth Sciences, NSF (EAR-1339051). The LA-ICP-MS instrument at the University of Rochester is partially supported by a grant from the Instrumentation and Facilities Program, Division of Earth Sciences, NSF (EAR- 1545637). We thank Mike Ackerson for insightful discussions. We thank Calvin Miller and William Collins reviews (and e-mail correspondence) on an earlier draft of this work. Thorough reviews by Matt Kohn and David London are much appreciated. We thank George Morgan for assistance with some of the CL images presented in this paper. The data presented in this paper can be found in the supporting information. The authors declare that there are no conflicts of interest.

References

Ackerson, M. R., N. D. Tailby, and E. B. Watson (2015), Trace elements in quartz shed light on sediment provenance, *Geochem. Geophys. Geosyst.*, *16*, 1894–1904, doi:10.1002/2015GC005896.
Acosta-Vigil, A., D. London, G. B. Morgan, and T. A. Dewers (2003), Solubility of excess alumina in hydrous granitic melts in equilibrium with peraluminous minerals at 700–800°C and 200 MPa, and applications of the aluminum saturation index, *Contrib. Mineral. Petrol.*, *146*, 100–119.
Breiter, K., L. Ackerman, M. Svojtka, and A. Muller (2013), Behavior of trace elements in quartz from plutons of different geochemical signature: A case study from the Bohemian Massif, Czech Republic, *Lithos*, *175–176*, 54–67.
Brooks, J. A. (1990), The petrogenesis of the Agamenticus complex and late paleozoic and mesozoic tectonics in New England, PhD thesis, Univ. of New Hampshire.
Cawthorn, R. G., and P. A. Brown (1976), A model for the formation and crystallization of corundum-normative calc-alkaline magmas through amphibole fractionation, *J. Geol.*, *84*, 467–476.
Chappell, B. W. (1999), Aluminum saturation in I- and S-type granites and the characterization of fractionated haplogranites, *Lithos*, *46*, 535–551.
Chappell, B. W., and P. R. Simpson (1984), Source rocks of I- and S-type granites in the Lachlan Fold Belt, southeastern Australia, *Philos. Trans. R. Soc. London A*, *310*, 693–707.
Chappell, B. W., and A. J. White, (1974), Two contrasting granite types, *Pac. Geol.*, *8*, 173–174.
Chappell, B. W., and A. J. R. White (2001), Two contrasting granite types: 25 years later, *Aust. J. Earth Sci.*, *48*, 489–499.
Chappell, B. W., A. J. R. White, and D. Wyborn (1987), The importance of residual source material (restite) in granite petrogenesis, *J. Petrol.*, *28*, 1111–1138.
Chappell, B. W., A. J. R. White, and I. S. Williams (1990), Excursion Guide B-1, Cooma Granidiorite and Berridale Batholith, in *Seventh International Conference on Geochronology, Cosmochronology, and Isotope Geology*, pp. 1–53, Bureau of Mineral Resources, Record 1990/50, Geology and Geophysics, Australia.
Chappell, B. W., A. J. R. White, and D. Wyborn (1993), The Cowra Granodiorite and its enclaves. Excursion guide, *Aust. Geol. Surv. Org. Rec. 67*, IAVCEI Canberra, Canberra.
Chappell, B. W., C. J. Bryant, A. J. Wyborn, A. J. R. White, and I. S. Williams (1998), High- and low-temperature I-type granites, *Resour. Geol.*, *48*, 225–235.
Chappell, B. W., C. J. Bryant, and D. Wyborn (2012), Peraluminous I-type granites, *Lithos*, *153*, 142–153.
Clemens, J. D., and V. J. Wall (1981), Crystallization and origin of some peraluminous (S-type granitic magmas, *Can. Mineral.*, *19*, 111–132.
Clemens, J. D., J. R. Holloway, and A. J. R. White (1986), Origin of an A-type granite: Experimental constraints, *Am. Mineral.*, *71*, 317–324.
Collins, W. J., S. D. Beams, A. J. R. White, and B. W. Chappell (1982), Nature and origin of A-type granites with particular reference to southeastern Australia, *Contrib. Mineral. Petrol.*, *80*, 189–200.
Compston, W., and R. T. Pidgeon (1986), Jack Hills, evidence of more very old detrital zircons in Western Australia, *Nature*, *321*, 766–769.
Daly, R. A. (1926), Geology of Ascutney Mountain, *U.S. Geol. Surv. Bull.*, *209*, 125 pp.
Dingwell, D. B., F. Holtz, and H. Behrens (1997), The solubility of H_2O in peralkaline and peraluminous granitic melts, *Am. Mineral.*, *82*, 434–437.
Eby, G. N., H. W. Krueger, and J. W. Creasy (1992), Geology, geochronology, and geochemistry of the White Mountain batholith, New Hampshire, in *Mesozoic Magmatism in Eastern North America*, edited by J. H. Puffer and P. Ragland, *Geol. Soc. Am. Spec. Pap.*, *268*, 379–397.
Ferris, J. P., and G. Ertem (1993), Montmorillonite catalysis of RNA oligomer formation in aqueous solution. A model for the prebiotic formation of RNA, *J. Am. Chem. Soc.*, *115*, 12,270–12,275.
Ferry, J. M., and E. B. Watson (2007), New thermodynamic models and revised calibrations for the Ti-in-zircon and Zr-in-rutile thermometers, *Contrib. Mineral. Petrol.*, *154*, 429–437.
Gerdes, A., P. Montero, F. Bea, G. Fershater, N. Borodina, T. Osipova, and G. Shardakova (2002), Peraluminous granites frequently with mantle-like isotope compositions: The continental-type Murzinka and Dzhabyk batholiths of the eastern Urals, *Int. J. Earth Sci.*, *91*, 3–19.
Griffin, T. J., A. R. White, and B. W. Chappell (1978), The Moruya batholith and geochemical contrasts between the Moruya and Jindabyne suites, *J. Geol. Soc. Aust.*, *25*, 235–247.
Gualda, G. A. R., M. S. Ghiorso, R. V. Lemons, and T. L. Carley, (2012), Rhyolite-MELTS: A modified calibration of MELTS optimized for silica-rich, fluid-bearing magmatic systems, *J. Petrol.*, *53*, 1–16.
Gulson, B. L., and P. C. Rankin (1977), Geochemical comparison of Woodlawn and Mount Painter acid volcanics, southeastern Australia, *J. Geol. Soc. Aust.*, *24*, 427–438.
Harrison, T. M., and M. M. Wielicki (2016), From the Hadean to the Himalaya: 4.4 Ga of felsic terrestrial magmatism, *Am. Mineral.*, *101*, 1348–1359.
Healy, B., W. J. Collins, and S. W. Richards (2004), A hybrid origin for Lachlan S-type granites: The Murrumbidgee Batholith example, *Lithos*, *78*, 197–216.
Hine, R., I. S. Williams, B. W. Chappell, and A. J. R. White (1978), Contrasts between I- and S-type granitoids of the Kosciusko Batholith, *J. Geol. Soc. Aust.*, *25*, 219–234.
Hopkins, M., T. M. Harrison, and C. E. Manning (2008), Low heat flow inferred from >4 Gyr zircons suggests Hadean plate boundary interactions, *Nature*, *456*, 493–496.
Joyce, A. S. (1973), Application of cluster analysis to detection of subtle variation in a granitic intrusion, *Chem. Geol.*, *11*, 297–306.
Kohn, M. J. (2014), Himalayan metamorphism and its tectonic implications, *Annu. Rev. Earth Planet. Sci.*, *42*, 381–419.
Kohn, M. J. (2016), Metamorphic chronology—A tool for all ages: Past achievements and future prospects, *Am. Mineral.*, *101*, 25–42.
Le Losq, C., D. R. Neuville, P. Florian, G. S. Henderson, and D. Massiot (2014), The role of Al^{3+} on rheology and structural changes in sodium silicate and aluminosilicate glasses and melts, *Geochim. Cosmochim. Acta*, *126*, 495–517.
London, D., G. B. Vi Morgan, and A. Acosta-Vigil (2012), Experimental simulations of anatexis and assimilation involving metapelite and granitic melt, *Lithos*, *153*, 292–307.
Medenbach, O. (1976), Geochemie der Elemente in Zirkon und ihre rämliche Verteilung—Eine Untersuchung mit der Elektronenstrahlmikrosonde, PhD thesis, Ruprecht-Karl-Univ., Heidelberg, Germany.
Miller, C. F. (1985), Are strongly peraluminous magmas derived from pelitic sedimentary sources?, *J. Geol.*, *93*, 673–689.
Miller, C. F. (1986), Comment on "S-type granites and their probable absence in southwestern North America", *Geology*, *14*, 804–805.
Morgan, G. B., D. London, and R. G. Luedke (1998), Petrochemistry of late miocene peraluminous silicic volcanic rocks from the morococala field, *J. Petrol.*, 39, 601–632.

Mysen, B., and B. Richet (2005), *Silicate Glasses and Melts: Properties and Structure. Developments in Geochemistry*, 525 pp., Elsevier Sci.
Mysen, B. O., and M. J. Toplis, (2007), Structural behavior of Al^{3+} in peralkaline, metaluminous, and peraluminous silicate melts and glasses at ambient pressure, *Am. Mineral.*, *92*, 933–946.
Mysen, B. O., D. Virgo, and I. Kushiro (1981), The structural role of aluminum in silicate melts—A Raman spectroscopic study at 1 atmosphere, *Am. Mineral.*, *66*, 678–701.
Neuville, D. R., L. Cormier, and D. Massiot, (2004), Al environment in tectosilicate and peraluminous glasses: A 27Al MQ-MAS NMR, Raman, and XANES investigation, *Geochim. Cosmochim. Acta*, *68*, 5071–5079.
Paces, J. B., and J. D. Miller (1993), Precise U-Pb ages of Duluth Complex and related mafic intrusions, northeastern Minnesota: Geochronological insights to physical, petrogenetic, paleomagnetic, and tectonomagmatic processes associated with the 1.1 Ga Midcontinent Rift System, *J. Geophys. Res.*, *98*, 13,997–14,013.
Patiño Douce, A. E. (1992), Calculated relationships between activity of alumina and phase assemblages of silica-saturated igneous rocks Petrogenetic implications of magmatic cordierite, garnet and aluminosilicate, *J. Volcanol. Geotherm. Res.*, *52*, 43–63.
Paton, C., J. Woodhead, J. Hellstrom, J. Hergt, A. Greig, and R. Maas (2010), Improved laser ablation U-Pb zircon geochronology through robust downhole fractionation correction, *Geochem. Geophys. Geosyst.*, *11*, Q0AA06, doi:10.1029/2009GC002618.
Paton, C., J. Hellstrom, B. Paul, J. Woodhead, and J. Hergt, (2011), Iolite: Freeware for the visualisation and processing of mass spectrometric data, *J. Anal. At. Spectrom.*, *26*, 2508–2518.
Pearce, N. J. G., W. T. Perkins, J. A. Westgate, M. P. Gordon, S. E. Jackson, C. R. Neal, and S. P. Chenery (1997), A compilation of new and published major and trace element data for NIST SRM 610 and NIST SRM 612 glass reference materials, *Geostand. Newsl.*, *21*, 115–144.
Phillips, G. N., V. J. Wall, and J. D. Clemens (1981), Petrology of the Strathbogie Batholigh: A Cordierite-bearing granite, *Can. Mineral.*, *19*, 47–63.
Puziewicz, J., and W. Johannes (1988), Phase equilibria and compositions of Fe-Mg-Al minerals and melts in water-saturated peraluminous granitic systems, *Contrib. Mineral. Petrol.*, *100*, 156–168.
Riebling, E. F. (1966), Structure of sodium aluminosilicate melts containing at least 50 mole% SiO_2 at 1500°C, *J. Chem. Phys.*, *44*, 2857–2865.
Shand, S. J. (1927), *The Eruptive Rocks*, 360 pp., D. Van Nostrand, New York.
Shearer, C. K., Jr., (1976), Geochemical and geological investigation of the Pawtuckaway Mountain plutonic complex, Rockingham County, New Hampshire, MS thesis, Univ. of New Hampshire.
Speer, J. A. (1984), Micas in igneous rocks, in *Reviews in Mineralogy*, vol. 13, edited by S. W. Bailey, pp. 299–356, Mineralogical Society of America, Washington, D. C.
Toplis, M. J., and D. B. Dingwell (2004), Shear viscosities of CaO-Al_2O_3-SiO_2 and MgO-Al_2O_3-SiO_2 liquids: Implications for the structural role of aluminium and the degree of polymerisation of synthetic and natural aluminosilicate melts, *Geochim. Cosmochim. Acta*, *68*, 5169–5188.
Toplis, M. J., D. B. Dingwell, and T. Lenci (1997a), Peraluminous viscosity maxima in Na_2O-Al_2O_3-SiO_2 liquids: The role of triclusters in tectosilicate melts, *Geochim. Cosmochim. Acta*, *61*, 2605–2612.
Toplis, M. J., D. B. Dingwell, K.-U. Hess, and T. Lenci (1997b), Viscosity, fragility and configurational entropy of melts along the join SiO_2-$NaAlSiO_4$, *Am. Mineral.*, *82*, 970–990.
Trail, D., S. J. Mojzsis, and T. M. Harrison (2007), Thermal events documented in Hadean zircons by ion microprobe depth profiles, *Geochim. Cosmochim. Acta*, *71*, 4044–4065.
Trail, D., J. B. Thomas, and E. B. Watson (2011), The incorporation of hydroxyl into zircon, *Am. Mineral.*, *96*, 60–67.
Trail, D., N. D. Tailby, A. Lanzirotti, M. Newville, J. T. Thomas, and E. B. Watson (2015), Magma redox evolution of silicic magmas: Insights from high spatial resolution Ce^{4+}/Ce^{3+} measurements of single Bishop Tuff zircons, *Chem. Geol.*, *402*, 77–88.
Valley, J. W., et al. (2005), 4.4 billion years of crustal maturation: Oxygen isotope ratios of magmatic zircon, *Contrib. Mineral. Petrol.*, *150*, 561–580.
Weiss, B. P., et al. (2015), Pervasive remagnetization of detrital zircon host rocks in the Jack Hills, Western Australia and implications for records of the early geodynamo, *Earth Planet. Sci. Lett.*, *430*, 115–128.
White, A. J. R., and B. W. Chappell (1983), Granitoid types and their distribution in the Lachlan Fold Belt, southeastern Australia, *GSA Mem.*, *159*, 21–34.
White, A. J. R., J. D. Clemens, J. R. Holloway, L. T. Silver, B. W. Chappell, and V. J. Wall (1986a), S-type granites and their probable absence in southwestern North America, *Geology*, *14*, 115–118.
White, A. J. R., J. D. Clemens, J. R. Holloway, L. T. Silver, B. W. Chappell, and V. J. Wall (1986b), Reply to comment on "S-type granites and their probable absence in southwestern North America", *Geology*, *14*, 805–806.
Wiedenbeck, M., et al. (2004), Further characterisation of the 91500 zircon crystal, *Geostand. Geoanal. Res.*, *28*, 9–39.
Williams, I. S., B. W. Chappell, Y. D. Chen, and K. A. W. Crook (1992), Inherited and detrital zircons—Vital clues to the granite protoliths and early igneous history of southeastern Australia, *Trans. R. Soc. Edinburgh Earth Sci.*, *83*, 503.
Wyborn, D., M. Owen, W. Compston, and I. McDougall (1982), The Laidlaw Volcanics a Late Silurian point on the geological time scale, *Earth Planet. Sci. Lett.*, *9*, 90–100.
Zen, E.-A. (1986), Aluminum enrichment in silicate melts by fractional crystallization: Some mineralogic and petrographic constraints, *J. Petrol.*, *27*, 1095–1117.